

Cyclic behavior of steel beam-concrete wall connections with embedded steel columns (II): Theoretical study

Guo-Qiang Li¹, Fulin Gu², Jian Jiang^{*1} and Feifei Sun¹

¹ State Key Laboratory for Disaster Reduction in Civil Engineering, Tongji University, Shanghai 200092, China

² College of Civil Engineering, Tongji University, Shanghai 200092, China

(Received October 05, 2016, Revised December 21, 2016, Accepted January 12, 2017)

Abstract. This paper theoretically studies the cyclic behavior of hybrid connections between steel coupling beams and concrete shear walls with embedded steel columns. Finite element models of connections with long and short embedded steel columns are built in ABAQUS and validated against the test results in the companion paper. Parametric studies are carried out using the validated FE model to determine the key influencing factors on the load-bearing capacity of connections. A close-form solution of the load-bearing capacity of connections is proposed by considering the contributions from the compressive strength of concrete at the interface between the embedded beam and concrete, shear yielding of column web in the tensile region, and shear capacity of column web and concrete in joint zone. The results show that the bond slip between embedded steel members and concrete should be considered which can be simulated by defining contact boundary conditions. It is found that the load-bearing capacity of connections strongly depends on the section height, flange width and web thickness of the embedded column. The accuracy of the proposed calculation method is validated against test results and also verified against FE results (with differences within 10%). It is recommended that embedded steel columns should be placed along the entire height of shear walls to facilitate construction and enhance the ductility. The thickness and section height of embedded columns should be increased to enhance the load-bearing capacity of connections. The stirrups in the joint zone should be strengthened and embedded columns with very small section height should be avoided.

Keywords: steel coupling beam; beam-to-wall connection; embedded steel column; failure mode; load-bearing capacity; close-form solution

1. Introduction

Steel coupling beams, taking the advantages of high strength, stiffness and energy-dissipation capacity, have attracted growing interests in the reinforced concrete shear wall systems (Fortney *et al.* 2007). Previous studies have generally focused on the coupling beams which are directly inserted into the wall (Harries *et al.* 1998, Kurama and Shen 2004, Shahrooz *et al.* 2004, Xuan *et al.* 2008, EI-Tawil *et al.* 2010, Eljadei 2012, Hung and Lu 2015, Chan-Anan *et al.* 2016). The energy is absorbed as the steel coupling beams undergo inelastic shear deformations and flexural hinges are formed at the bottom of wall piers (Shi *et al.* 2013). To ensure the energy-absorbing capability of steel coupling beams, a reliable connection between the steel coupling beam and concrete shear wall is essential. It is recognized that the connection is always subjected to brittle failure and a sufficient embedding length should be guaranteed to ensure the complete load transfer from the coupling beam to the shear wall (Park and Yun 2006a, Zhu 2008, Hosseini *et al.* 2011, Nie *et al.* 2014, Gholhaki and Ghadaksaz 2016). Recently, Eljadei and Harries (2014) proposed a performance design of coupled shear wall

systems which were transformed from a coupled core wall system to a system of linked wall piers systems. This was based on the assumption that the damage of coupling beams occurred prior to the plastic capacity of the system. Morelli *et al.* (2016) investigated the seismic behavior of two types of coupling beams with beam splices at the middle and end of the beam. It was found that the failure occurred at the beam splice due to the tearing of the web or the bolt hole. Bengar and Aski (2016) found that the coupled shear wall systems with steel coupling beams had better ductility and energy dissipation capacity than that of RC beams. The results showed that the latter. Traditional steel beam-to-wall connections have high stiffness to effectively transfer the shear forces between coupling beam and wall, but have low ductility and suffer from severe strength degradation (ASCE 2010).

To improve the performance of hybrid coupled shear walls and enhance its construction efficiency, a new detailing of connections between steel coupling beam and concrete shear wall is proposed in this paper, as shown in Fig. 1. A steel bracket, welded to the flange of the imbedded column, projects beyond the face of the concrete shear wall and connects to the steel coupling beam through an extended bolted connection. The coupling beam is thus replaceable, which facilitates and accelerates the restoration after major earthquakes. There are rare studies on steel coupling beam-concrete shear wall connection with

*Corresponding author, Ph.D.,
E-mail: jiangjian_0131@163.com

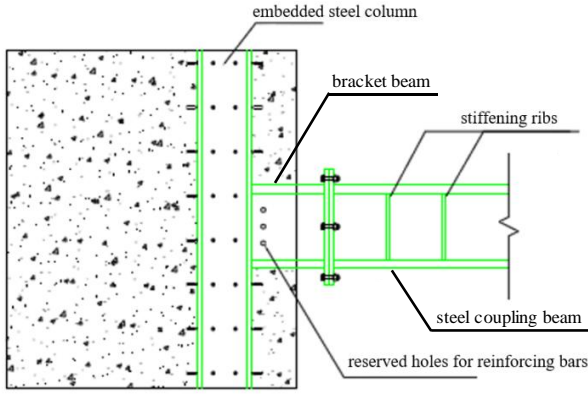


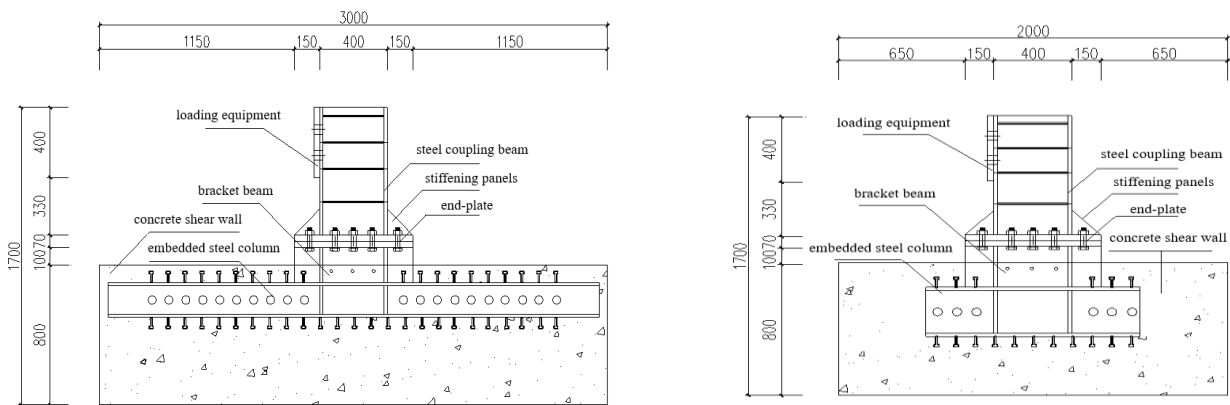
Fig. 1 Schematic of connections between steel coupling beam and concrete shear wall with embedded steel columns

embedded steel columns.

This paper theoretically investigated the mechanical behavior and failure mode of the connection between steel coupling beams and shear walls by means of embedded steel columns. The influence of the length of embedded steel columns was studied. Finite element models of the proposed connections with embedded steel columns were built in ABAQUS, and were validated against experimental results. Parametric studies were carried out to investigate the influence of dimension and location of embedded columns on the performance of connections. Based on the experimental and numerical studies, a close-form solution of the load-bearing capacity of connections was finally proposed. The theoretical results were compared with experimental and numerical results.

2. Brief description of experiments

The detailed layout and results of tests were presented in a companion paper by the authors (Li *et al.* 2016). Fig. 2 shows the details of the tested connections with short (1100 mm) and long (2900 mm) embedded steel columns. Dimensions of two of the tested specimens are listed in Table 1.



(a) Long embedded steel column

(b) Short embedded steel column

Fig. 2 Layout of the tested connections with short and long embedded columns (all units in mm)

Table 1 Parameters of specimens (units: mm)

No. of specimens	Type of columns	Size of walls (height × thickness × width)	Length of columns	Loading
DJ	Short column	800×300×3000	1100	Monotonic
DW	Short column	800×300×3000	1100	Cyclic
CJ	Long column	800×300×2000	2900	Monotonic
CW	Long column	800×300×2000	2900	Cyclic

3. Numerical modeling and validation

3.1 Finite element modeling

The 8-nodes 3D solid element, C3D8R, was used for structural steel members, concrete shear walls and the end-plate with bolts. The 2-nodes linear truss element, T3D2, was used for modeling reinforcing bars. To improve the accuracy and efficiency of simulation, a fine mesh was used for the joint panel, and a relatively coarse mesh for other regions, especially the supporting beam and steel coupling beam. The FE models of the specimens DJ and CJ are shown in Fig. 3. The shear wall was fixed on the supporting beam.

The bilinear kinematic hardening model of Mises yielding criteria and related flow rules were used for all steel members and reinforcement. The material properties of steel were taken from the uniaxial tensile tests. The yield strengths of steel beams, embedded columns, reinforcements, stirrups were 284 MPa, 329 MPa, 557 MPa and 317 MPa, respectively. Their ultimate strengths were 442 MPa, 480 MPa, 573 MPa, 535 MPa, respectively. The Young’s modulus of steel was taken as 200 GPa. High strength grade10.9 friction-grip bolts were used for the beam-to beam connection. The 28-day compressive strength of

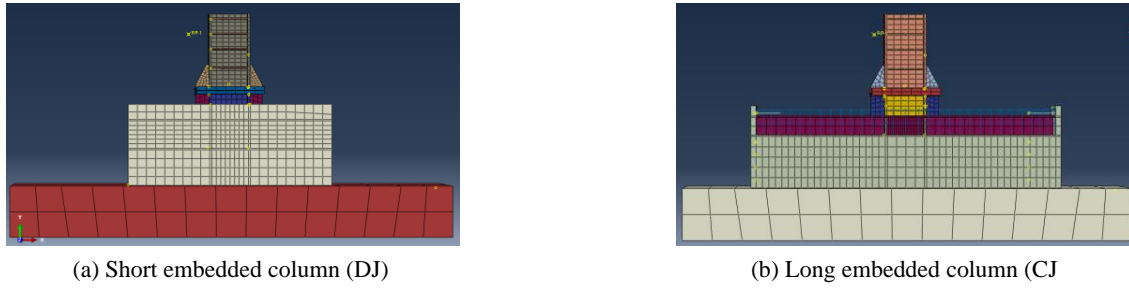


Fig. 3 The FE model of the tested connections with short and long embedded columns

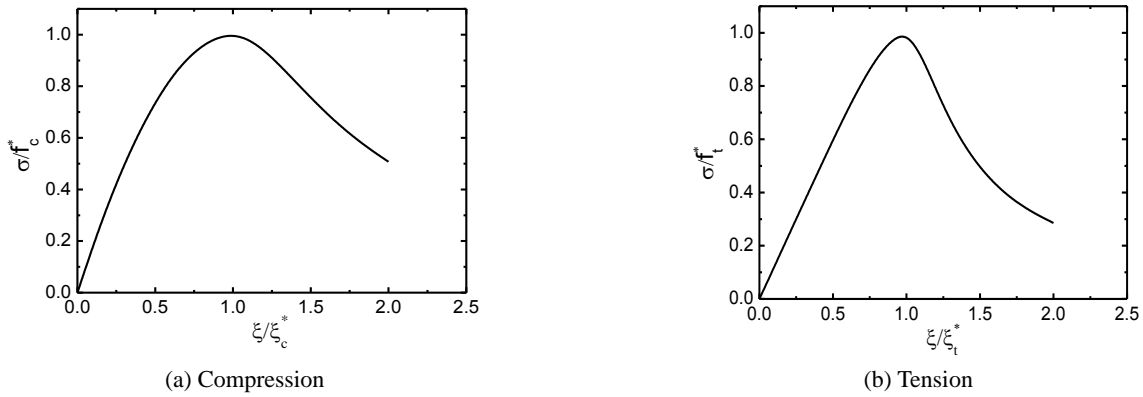


Fig. 4 Stress-strain relationship of concrete



Fig. 5 Predicted stress distribution in steel members and reinforcement at failure of specimens

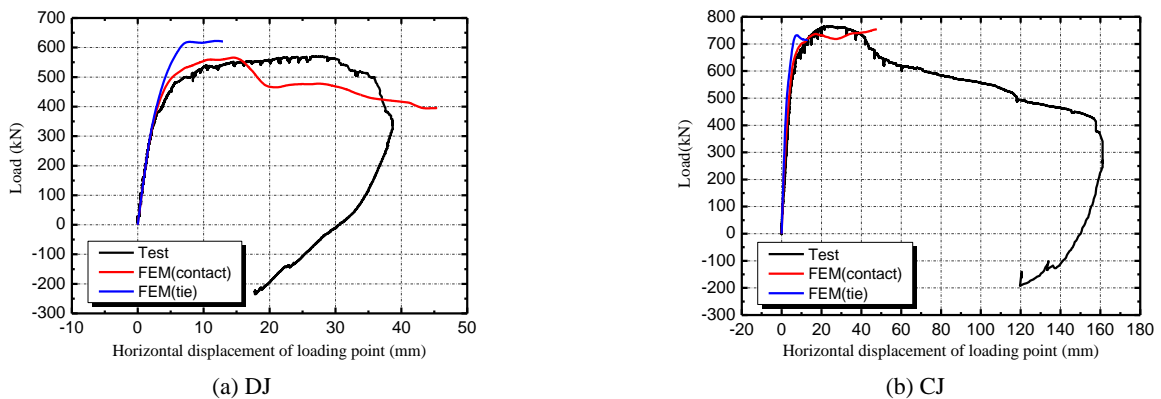


Fig. 6 Comparison of measured and predicted load-displacement curves for the specimens

concrete was 30.1 MPa. The stress-strain relation of concrete was based on GB (2010), as shown in Fig. 4. The damage plastic model in ABAQUS was used for concrete (Zhang *et al.* 2008, Ren and Li 2015).

Two types of bond relation between embedded steel members and concrete were considered in this study: (1) no bond slip was considered by using “tie”; (2) consider the friction sliding by using face-to-face “contact”. The bond

relation is used to simulate the shear resistance provided by shear studs placed on the flanges of embedded column. A friction coefficient should be defined for the tangential contact between the embedded steel member and concrete. The friction coefficient mainly depends on the arrangement of the shear studs on the flanges of the column. The short and long embedded columns have different number of studs and thus different friction coefficients. Two friction coefficients of 0.25 and 1.0 were used for the short and long embedded column, respectively. They were determined by parametric studies in which the same stiffness of the connection was ensured by comparing the predicted and measured load-displacement curve, as shown in Fig. 6. The separation of embedded steel members and concrete was allowed in the normal direction. The reinforcement was embedded in the concrete (i.e., share the same nodes with the concrete wall) and thus no bond slip between reinforcement and concrete was considered.

3.2 Validation against test results

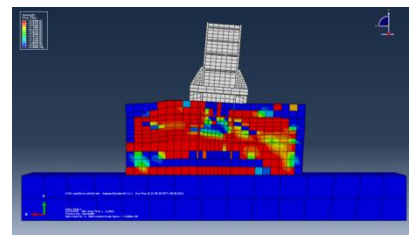
The stress distributions in the steel members and reinforcement for the specimens DJ and CJ at failure are shown in Fig. 5. The yielding part is in red and elastic state is in blue. The failure modes for the short and long-column connections were different. For the short-column connection (DJ), the steel column remained elastic and the vertically distributed reinforcement in the tension side first yielded (Fig. 5(a)). The yielding of reinforcement was caused by the rigid rotation of steel column resulting from a short anchorage length and thus high flexural stiffness. The long-column connection CJ failed due to the shear yielding of the web of the embedded column in the joint panel, followed by the yielding of the column web and reinforcement in the tension side (Fig. 5(b)). The premature shear yielding of the column web was attributed to the S-shape deformation of the embedded long column due to its small flexural stiffness.

Fig. 6 shows the comparison of measured and predicted load-displacement curves for the specimens DJ and CJ. The effect of bond slip between embedded steel members and concrete using the “Tie” and “Contact” was studied. In general, these two types of bond conditions produced similar results for the ultimate load-bearing capacity of connections. The predicted load-bearing capacity from the tie bond was larger than that from the contact bond. The increased capacity was due to the higher stiffness in the tie bond model than the reality since the tie bond cannot simulate the slip between steel members and concrete. This slip became more severe after the cracking of the wall. The contact bond can capture the slip and thus gave a better agreement with the test results. The descent stage of load-displacement curves depended on the softening part of the constitutive model, especially the complex concrete damage and slip between reinforcement and concrete. This is beyond the scope of this paper. The comparison of observed and predicted failure model of the specimen DJ and CJ is shown in Figs. 7 and 8, respectively. For the specimen DJ as shown in Fig. 7, a through crack formed along the interface between embedded column and concrete, extending from the left top to the right, which was also predicted by the numerical model. The cracking in the long-column connection (Fig. 8) was concentrated in the tension side and the numerical prediction agreed well with the test observation. Therefore, the tension contour of concrete in ABAQUS can reasonably represent the practical cracking pattern of the shear wall, and thus the FE model is capable of reasonably simulating the mechanical behavior of shear walls.

Table 2 summaries the test and numerical results of load-bearing capacities of the connections. For the specimens DJ and CJ, the numerically predicted bearing capacities were 592 kN and 732 kN, respectively, compared to measurements of 569 kN and 765 kN. Good agreement was obtained since the errors were within 5%.



(a) Test

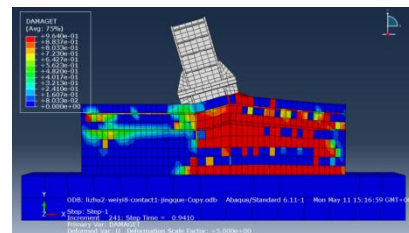


(b) Numerical analysis

Fig. 7 Comparison of measured and predicted cracking pattern of the specimen DJ



(a) Test



(b) Numerical analysis

Fig. 8 Comparison of measured and predicted cracking pattern of the specimen CJ

Table 2 Comparison of measured and predicted load-bearing capacities of connections

Specimen	Bearing capacity from test (kN)	Bearing capacity of FEM (contact) (kN)	Absolute error
DJ	569	592	3.9%
CJ	765	732	4.3%

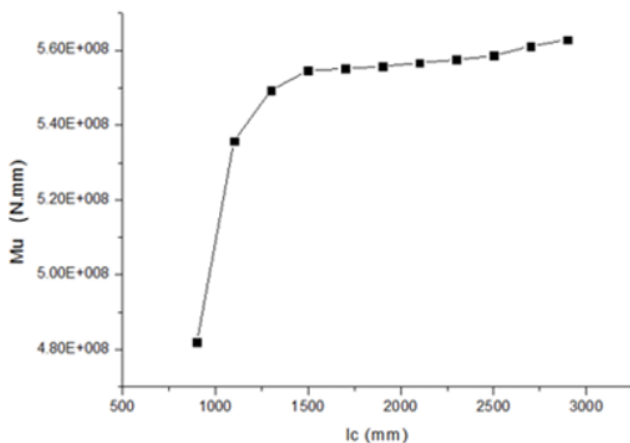
Table 3 Variation of influencing factors (all units in mm)

No.	L_c	d_c	b_f	h_f	t_f	t_w
1	900~2900	100	200	200	8	14
2	2900	100~300	200	200	8	14
3	2900	100	100~300	200	8	14
4	2900	100	200	100~400	8	14
5	2900	100	200	200	8~24	14
6	2900	100	200	200	8	6~14

4. Parametric study

To further study the mechanical behavior of the proposed connection, parametric studies were conducted by varying the dimension and location of embedded steel columns. The influencing factors and their variation range are listed in Table 3. These included the column length (900 mm ~ 2900 mm), embedment depth (100 mm ~ 300 mm), flange width (100 mm ~ 300 mm), section height (100 mm ~ 400 mm), flange thickness (8 mm ~ 24 mm) and web thickness (6 mm ~ 14 mm) of embedded columns. Only one parameter was changed with others kept constant.

For a convenient comparison between theoretical predictions and test measurements hereafter, the moment resistance of the connection was used instead of ultimate loads. This is because the load-bearing capacity of the connection deduced in Section 5 was in a form of bending moment resistance. The moment resistances of the specimens were calculated from the measured force-displacement curves (by multiplying the force with the length of the cantilever coupling beam).

Fig. 9 Variation of load-bearing capacity of connections against L_c

4.1 Influence of column length L_c

Fig. 9 shows the variation of load-bearing capacity of the connection against the length of the embedded column L_c . The load-bearing capacity increased as the column length increased. There was an obvious cut-off point on the curve. The increasing rate of load-bearing capacity for $L_c > 1500$ mm was far smaller than that for $L_c < 1500$ mm. The different rates can be explained by different failure modes for the connections with short and long embedded columns. For longer columns (greater than a certain critical length), the shear capacity of column web in the joint panel governed the ultimate bearing capacity of the connection. While for shorter columns, the column web remained elastic and experienced rigid rotation, and thus the failure of connection was governed by the yielding of reinforcement in the tensile side around the column.

4.2 Influence of column length d_c

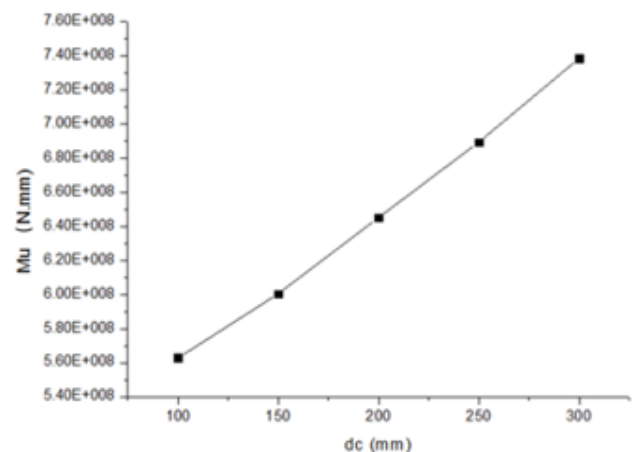
Fig. 10 shows the linear variation of load-bearing capacity of connections with the embedment depth of columns d_c . The deeper the embedded column, the larger compression area of the interface between the bracket beam and concrete, and thus the higher load-bearing capacity of connections.

4.3 Influence of section dimension (b_f , t_f , h_w , t_w)

The variations of load-bearing capacity of connections against the dimensions (b_f , t_f , h_w , t_w) of column cross-section are shown in Fig. 11. The load-bearing capacity of connections was sensitive to the height of the column web followed by the flange width and web thickness. The flange thickness of columns had little effect given differences of 3%.

5. Analytical study

This section presents the analytical model of the load-bearing capacity of connections between steel coupling beam and shear wall with long embedded steel columns (which shows better load-bearing capacity than that with

Fig. 10 Variation of load-bearing capacity of connections against d_c

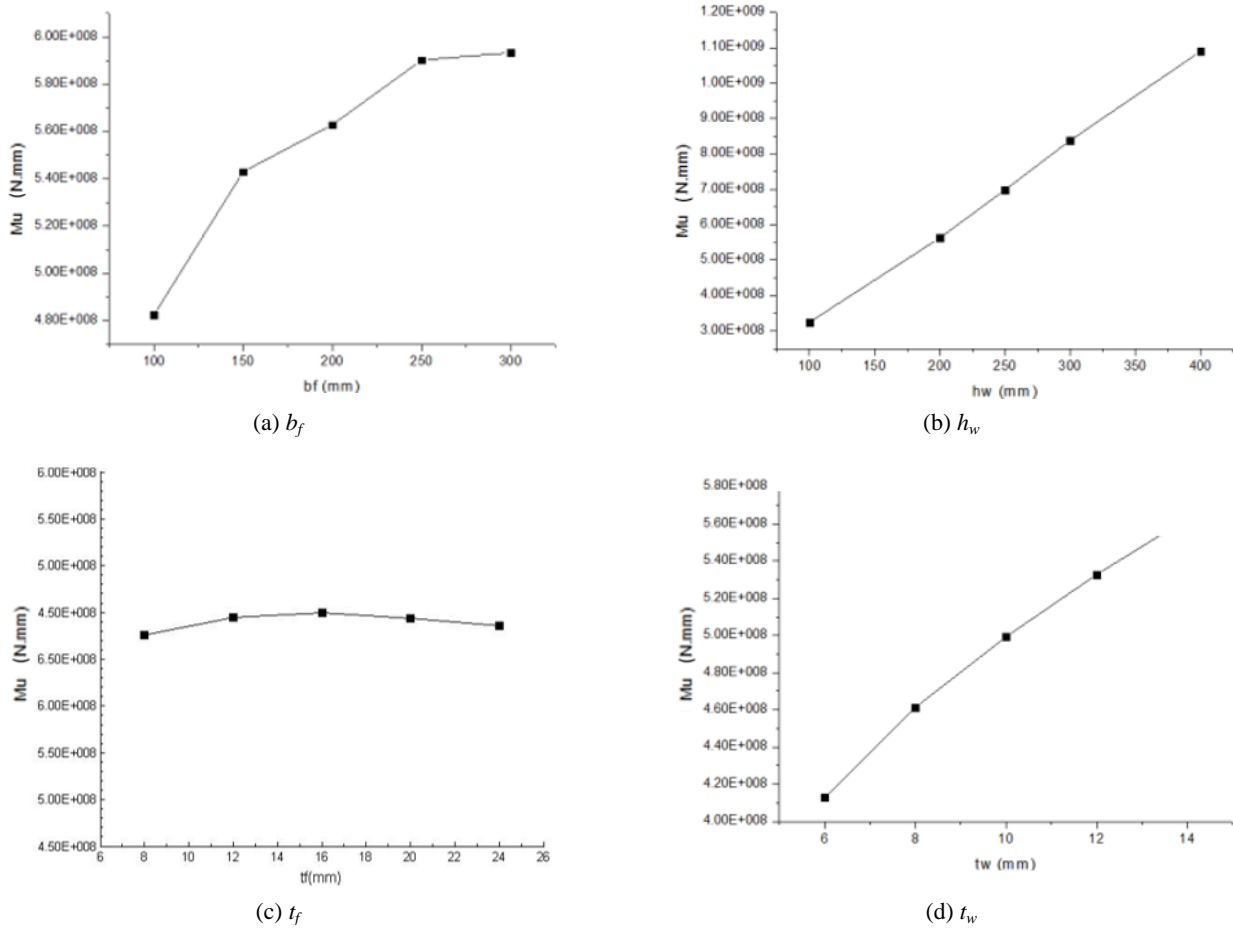


Fig. 11 Variation of load-bearing capacity of connections against the size of cross-section of columns

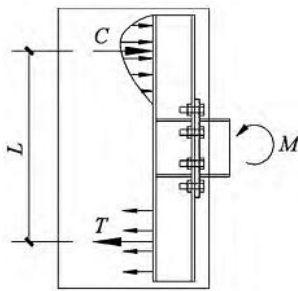


Fig. 12 Schematic of load transmission by Wu *et al.* (2014)

short column). Wu *et al.* (2014) proposed a mechanical model for determining the load-bearing capacity of long-column connections, as shown in Fig. 12. The moment was resisted by a couple of opposite and equal forces: compression provided by concrete (C) and tension by reinforcing bars (T). The flexural capacity can be calculated by the product of the force and predefined arm. However, this model did not consider the contribution of concrete in the joint zone and shear capacity of column web to the load-bearing capacity of connections. No calculation formula was provided for the determination of tension T or compression C . In addition, for connections with embedded steel



Fig. 13 Failure modes for RCS connections by Sheikh *et al.* (1989)

column, the tension or compression will not reach their yielding strength at the failure of the connection due the strong anchorage of the column.

The steel beam-to-concrete wall connection proposed in this study is similar to RC columns–steel beam (RCS) connections. Sheikh *et al.* (1989) conducted a series of experiments on 15 RCS connections (7 monotonic loading tests and 8 cyclic loading tests). Two failure modes were found (Fig. 13): shear failure caused by the yielding of steel beam web and shear failure of concrete in the joint zone, and bearing failure due to the crushing of concrete around the steel beam flange and column. The proposed beam-to-wall connection shows some differences from RCS connections. Firstly, only one side of the wall suffers from the load transmitted by the steel coupling beam. Secondly, the thicknesses of concrete on two sides of embedded steel column are different. These two differences may result in the residual strength of connection after the crushing of concrete near the coupling beam, and different stiffness and strength of the compression and tension regions. This facilitates the yielding of reinforcement in the tension region. Therefore, the failure mode of shear yielding of steel column web together with concrete bearing failure was assumed in this study for connections with long embedded columns.

5.1 Assumptions for mechanical analysis

The following assumptions were made to determine the load-bearing capacity of connections:

- (1) Only the compressive strength and shear strength of concrete were taken into account (the tensile strength was ignored);
- (2) The concrete around the flange of embedded steel coupling beam reached its compressive strength and rectangular stress block was assumed;
- (3) The shear force V_b transmitted by steel coupling beams was resisted by a combination of two parts (Eq. (1)): compressive force V_{dc} provided by concrete around the embedded coupling beam and shear resistance V_{sd} afforded by headed studs along

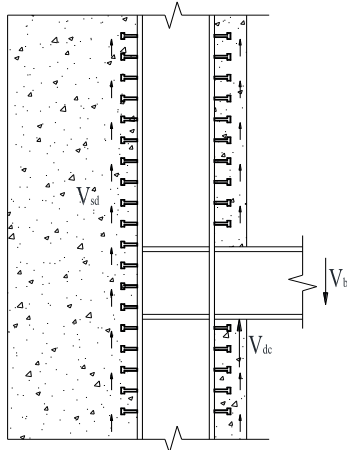


Fig. 14 Schematic of shear force transmission in the connection

the embedded steel column flange (Fig. 14). The direction of V_{sd} should be determined by the force equilibrium equation. The strength of shear stud should be checked to avoid the anchorage failure based on design requirements.

$$V_b = V_{dc} + V_{sd} \quad (1)$$

- (4) For both steel beam and embedded column, the shear force was resisted by their web while the moment was resisted by flanges. Compressive and tensile forces P_b formed at the flanges of embedded beams can be calculated by Eq. (2). As shown in Fig. 16, M_b represents the moment at the joint zone caused by the shear force V_b in the coupling beam; M_{dc} denotes the moment resisted by compression force V_{dc} in the concrete along the embedment distance; M_b' represents the moment at the interface between steel column and beam.

$$P_b = \frac{M_b'}{h_b}, M_b' = M_b - M_{dc} \quad (2)$$

5.2 Formula for the load-bearing capacity of connection

The simplified mechanical model and dimension of members are shown in Fig. 15. The section height, web height, flange thickness of steel coupling beam are represented by h_b , $h_{b0} = h_b - 2 \cdot t_{fb}$, respectively. The section height, web height, flange thickness of the embedded column are denoted by h_c , $h_{c0} = h_c - 2 \cdot t_f$, t_{fb} , respectively. The embedment distance of steel column from the edge of the wall is d_c , and the thickness of shear wall is t_q . The beam and column have the same the flange width b_f . The b_i represents the thickness of concrete within the half flange of embedded steel column while b_o represents the distance between the external edges of steel column and reinforcing cage.

Fig. 16 shows the schematic of mechanical analysis and deformation of the proposed connection. The sufficient anchorage of the long embedded column prevented the rigid

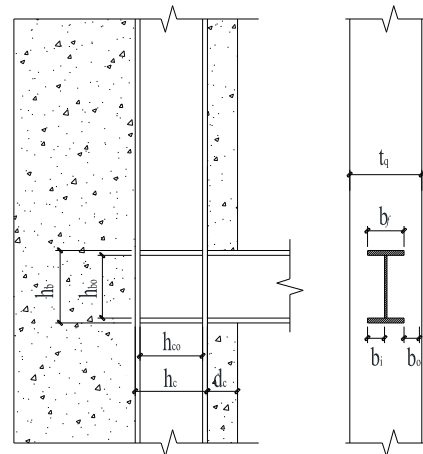


Fig. 15 Dimensions of the proposed connection with embedded steel columns

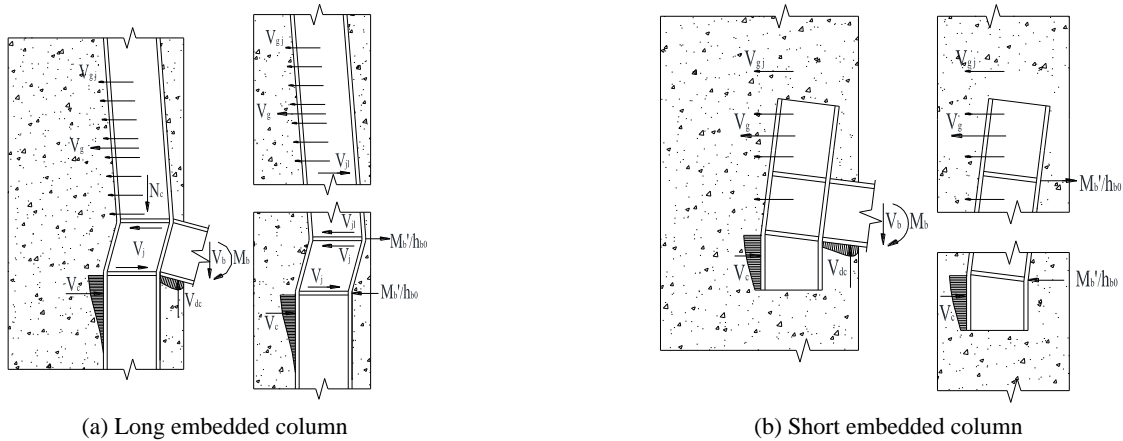


Fig. 16 Schematic of mechanical model of connections with different lengths of embedded columns

rotation of column as shown in Fig. 16(a). On the contrary, if the column section connected to the beam had insufficient shear resistance V_{gj} as well as the shear yielding of column web and shear failure of concrete in the joint zone, plastic hinges may form and plastic rotation of the connection occurred, as shown in Fig. 16(b). The load-bearing capacity of the connection can be expressed as

$$\frac{M'_b}{h_b} = V_{jl} + V_j \quad (3)$$

where V_{jl} represents the shear capacity of tensile region of the connection; V_j represents the shear capacity of joint panel zone.

In summary, there are three components for the moment resistance of the connection:

- (1) Moment resistance M_{dc} provided by concrete in compression within the embedment distance d_c of steel beam;
- (2) Moment resistance M_c provided by shear yielding of reinforcement within column length in the tensile column web in the tensile region or yielding of all side;
- (3) Moment resistance M_j offered by the shear yielding of column web and shear failure of concrete in joint zone.

The ultimate bending capacity of the proposed connection is expressed in Eq. (4) as

$$M_u = M_{dc} + M_c + M_j \quad (4)$$

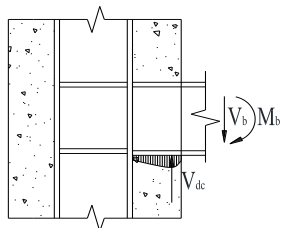


Fig. 17 Schematic of stress distribution in the concrete for calculating M_{dc}

The test results showed the crushing and spalling of concrete at the interface of wall and embedded steel beam at the failure of connections. Therefore, it was assumed that the concrete reached its compressive strength. The stress distribution in concrete along the embedment length was simplified to equivalent rectangular stress block, as shown in Fig. 17. The depth of the stress block “ x ” was taken as d_c multiplied by β_1 (GB 2010, Park and Yun 2005). The moment M_{dc} caused by this compressive stress block along the rotation center is expressed in Eq. (5) as

$$M_{dc} = \beta_1 \cdot \left[\left(1 - \frac{\beta_1}{2} \right) \cdot d_c \cdot b_f \cdot d_c \right] \cdot f_b \quad (5)$$

where f'_c is the compressive strength of concrete; f_b is the bearing strength of concrete which depends on the width of steel coupling beam b_f and the thickness of shear wall t_q . The method by Kriz and Raths (1965) was used in this study to determine f_b as

$$f_b = 4.5 \cdot \sqrt{f'_c} \cdot \left(\frac{t_q}{b_f} \right)^{0.60} \quad (6)$$

Calculation of M_c

The FE analysis showed two failure modes of connections with long embedded column. If the shear strength of column web was large enough that all reinforcement within column length on the tensile side yielded. Otherwise, shear yielding failure of column occurred.

Fig. 18 shows the mechanical model for determining shear strength the tensile part of the joint. The parameters V_c , V_{gj} , V_{jl} represent the resultant yielding force of all reinforcing bars within column length, shear strength of column web, shear capacity of tensile region of the connection, respectively. The V_{jl} was taken as the minimum value of V_g , V_{gj} as in Eqs. (7) and (8)

$$V_{jl} = V_g, \quad \text{if } V_{gj} > V_g \quad (7)$$

$$V_{jl} = V_{gj}, \quad \text{if } V_{gj} < V_g \quad (8)$$

The parameters V_{gj} and V_g can be calculated as

$$V_{gj} = 0.58 \cdot f_y \cdot h_{c0} \cdot t_w \quad (9)$$

$$V_g = \frac{(L_c - H_b)}{s} \cdot f_{vy} \cdot A_{vs} \quad (10)$$

Where t_w is the thickness of steel column web; f_y is the yield strength of column web; H_b is the section height of steel coupling beam; A_{vs} is the area of single vertical distributed reinforcing bar in shear wall; s is the spacing of reinforcing bars; f_{vy} is the yield strength of reinforcing bars.

As the embedded steel column is usually placed along the entire height of shear wall, it is not likely for the occurrence of the yielding of all reinforcement in the wall. In this study, only the shear yielding of column web was considered and thus M_c can be calculated by Eq. (11) as

$$M_c = V_{jl} \cdot h_b \quad (11)$$

Calculation of M_j

Based on the research on RCS connections (Parra-Moniesinos and Wight 2001, Shen 2007, Zhang 2008), a new model to determine M_j was proposed according to the shear deformation of the joint panel. There are three mechanisms contributing to the shear strength of the joint panel (Fig. 19): (a) column web mechanism; (b) inner strut mechanism from concrete; (c) outer truss mechanism from stirrups. The shear capacity of the connection V_j is expressed in Eq. (12) as

$$V_j = V_{wh} + V_{jc} + V_{jo} \quad (12)$$

Thus

$$M_j = V_j \cdot (h_b - t_{fb}) \quad (13)$$

where M_j is the flexural capacity of the joint panel; V_{wh} is the shear strength of steel column web in the joint panel; V_{jc} is the shear capacity of concrete through inner strut mechanism in the joint panel; V_{jo} is the shear capacity through outer strut mechanism in the joint panel.

(a) Calculation of V_{wh}

Previous studies showed a non-uniform distribution of strain in the joint panel of steel beam-concrete column connection (Parra-Moniesinos and Wight 2001), as shown in Fig. 20(a). Test results showed that after yielding the ultimate shear strain exceeded over 60% of the steel web panel width for exterior joints (Parra-Moniesinos and Wight 2001, Zhang 2008). A trapezoidal distribution of shear stresses was thus assumed, as shown in Fig. 20(b). The shear strength of the steel web panel can be expressed as

$$V_{wh} = k_w \cdot \frac{f_y}{\sqrt{3}} \cdot h_{c0} \cdot t_w \quad (14)$$

where $k_w = 0.8$ is a reduction coefficient.

(b) Calculation of V_{jc}

The test results on RCS connections showed that the connection remained elastic before its cracking. The concrete in the panel zone resisted most of shear forces. As the load increased, there developed diagonal cracking and formed strut mechanism, which was similar to the RC connections. Due to the confining of the flanges, stiffening ribs and stirrups, the shear capacity of RCS connections was much greater than that of traditional reinforced concrete connections. According to the inner strut model shown in Fig. 21, the shear capacity of concrete in the joint zone was expressed as (Zhang 2008)

$$V_{jc} = 0.6v_{ibase} f'_c (-0.0048f'_c + 1.13)k_1 h_{c0} b_i \quad (15)$$

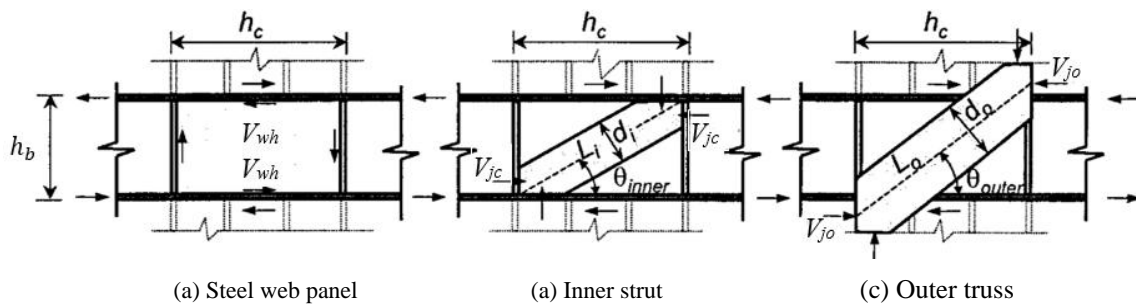


Fig. 19 Mechanisms contributed to the shear capacity of joint panel for calculating V_j

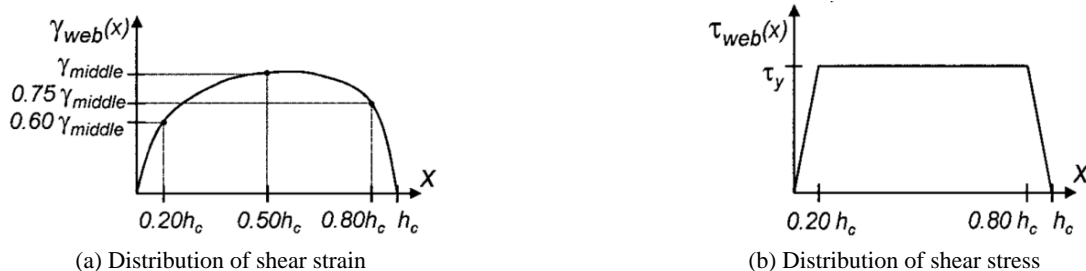


Fig. 20 Distribution of strains and stresses in the column web panel (Parra-Moniesinos and Wight 2001)

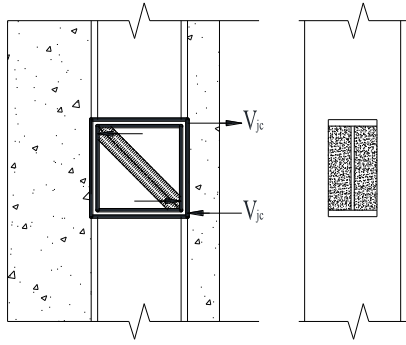


Fig. 21 Shear mechanism for inner strut model

$$b_i = \frac{(b_f - t_w)}{2} \quad (16)$$

Where v_{ibase} is basic strength factor for inner strut, $v_{ibase} = 1.0$; k_1 is a coefficient related to the configuration of connections, $k_1 = 1.0$.

(c) Calculation of V_{jo}

For reinforced concrete connections, stirrups play an

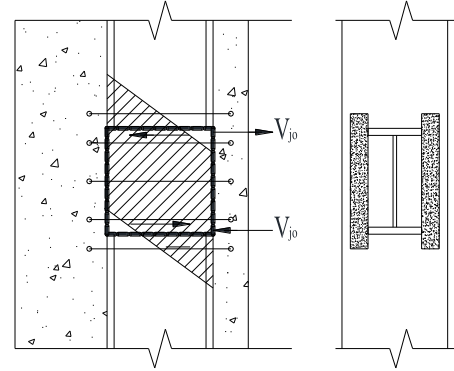


Fig. 22 Shear mechanism for outer truss model

important role in improving the seismic performance of connections by directly resisting shear load, confining core concrete in the joint zone and preventing buckling of longitudinal reinforcing bars. Previous experiments on RCS connections showed that stirrups usually yielded after the shear yielding of column web panel and induced large deformation. However, for the ultimate limit state, stirrups can still yield. Fig. 22 shows the outer truss mechanism

Table 4 Comparison of load-bearing capacity of connections between numerical results and close-form solution

No.	L_c (mm)	d_c (mm)	t_q (mm)	b_f (mm)	h_c (mm)	t_f (mm)	t_w (mm)	Ultimate displacement (mm)	Ultimate capacity (kN)	FEM results (kN·m)	Formula results (kN·m)	Difference (%)
1	2500	300	400	300	400	16	6	7.1	919	735	850	13.5
2	2500	250	400	250	300	18	8	7.0	834	626	643	2.7
3	2500	200	400	200	250	20	10	6.3	726	508	513	1.0
4	2500	150	400	150	200	22	12	8.0	645	420	399	-4.9
5	2500	100	400	100	100	24	14	11.6	415	250	227	-9.3
6	2300	300	400	250	250	22	14	7.7	918	735	719	-2.2
7	2300	250	400	200	200	24	6	5.6	606	455	403	-11.4
8	2300	200	400	150	100	16	8	5.7	412	288	223	-22.6
9	2300	150	400	100	400	18	10	21.1	758	554	572	3.1
10	2300	100	400	300	300	20	12	14.2	948	559	557	-0.4
11	2100	300	400	200	100	18	12	6.1	572	458	405	-11.5
12	2100	250	400	150	400	20	14	17.4	928	775	808	4.2
13	2100	200	400	100	300	22	6	14.1	578	423	414	-2.2
14	2100	150	400	300	250	24	8	5.5	719	467	444	-5.0
15	2100	100	400	250	200	16	10	5.8	646	388	367	-5.3
16	1900	300	400	150	300	24	10	8.9	784	629	619	-1.7
17	1900	250	400	100	250	16	12	9.5	655	512	499	-2.4
18	1900	200	400	300	200	18	14	6.9	790	553	4.96	-10.3
19	1900	150	400	250	100	20	6	4.5	401	260	213	-18.1
20	1900	100	400	200	400	22	8	8.5	896	539	527	-2.2
21	1700	300	400	100	200	20	8	7.9	570	457	440	-3.7
22	1700	250	400	300	100	22	10	5.9	561	421	329	-21.8
23	1700	200	400	250	400	24	12	9.5	106	746	744	-0.3
24	1700	150	400	200	300	16	14	8.2	927	592	572	-3.4
25	1700	100	400	150	250	18	6	5.7	559	336	309	-8.1

produced by stirrups. Based on JGJ (2002), the same calculation of shear capacity of stirrups as reinforced concrete connections was used for RCS connections. The shear capacity V_{jo} was determined as

$$V_{jo} = 0.9 \cdot f_{yv} \cdot \frac{A_{sv}}{s} \cdot (h_b - t_{fb}) + 0.4 \cdot \sqrt{f_c'} \cdot b_o \cdot h_c \quad (17)$$

Substituting Eqs. (5), (11) and (13) into Eq. (4) yields the load-bearing capacity of connections with embedded steel column as

$$Mu = \beta_1 \cdot \left[\left(1 - \frac{\beta_1}{2} \right) \cdot d_c \cdot b_f \cdot d_c \right] \cdot f_b + V_{jl} \cdot h_b + V_j \cdot (h_b - t_{fb}) \quad (18)$$

The above determination of the load-bearing capacity of the connection between the embedded column and coupling beam is based on the observed failure mode in the test conducted by the authors. In the test, a weak connection was designed and tested to ensure that failure occurred at the connection. In practice, the connection should be over designed based on the predicted load-bearing capacity in this study to concentrate the failure at the coupling beam. In this way, the coupling beam will yield and dissipate considerable seismic energy.

5.3 Validation against test results

The proposed analytical solution was first validated against test results of CJ. If the yielding strength was used in the calculation, a smaller load-bearing capacity (554 kN·m) was obtained than the test results (613 kN·m) with an error of nearly 10%. While by using ultimate strength as an alternative, the predicted bearing capacity increased to 622 kN·m and the error was reduced to 1.4%, which shows good agreement with test results. This indicates that the steel column web has entered hardening stage when the connection reaches its ultimate bearing capacity.

5.4 Verification against FE results

The accuracy of the proposed closed-form solution was further verified against FE results by varying the length of embedded column L_c , embedment depth d_c , flange width b_f , section height h_c , flange thickness t_f and web thickness t_w . The comparison was listed in Table 4. The theoretical results agreed well with the numerical results since the differences of most cases are within 10%. The large differences of about 20% for cases 8, 19, 22 were due to the relatively small section height of steel columns that flexure failure was easy to take place. This dimension of embedded columns should be avoided.

6. Conclusions

This paper theoretically studied the cyclic behavior of hybrid connections between steel coupling beams and concrete shear walls with embedded steel columns. Parametric studies were carried out using finite element models to figure out the key influencing factors. The

closed-form solution of load-bearing capacity of the proposed connection was deduced and compared with experimental and numerical results. The conclusions may be drawn as follows:

The contact boundary condition should be used in the FE model to simulate the bond slip between embedded steel members and concrete, which shows better stiffness of connections.

Two failure modes were found for connections with embedded steel columns in different lengths. The connection with long embedded columns under cyclic loads failed due to the shear yielding of column web in the joint panel while that with short columns failed by the yielding of reinforcement restraining the embedded column due to its rigid rotation.

The section height of the embedded column played a key role in the load-bearing capacity of connections. The flange width and web thickness of columns also have significant effects.

The close-form solution of bending strength of the connection was proposed by considering three contributions from the compressive strength of concrete at the interface between embedded beam and concrete, shear yielding of column web in the tensile region, and shear capacity of column web and concrete in joint zone.

The accuracy of the proposed solution of load-bearing capacity was validated against experimental results with an error of 1.4%, and verified against FE results with differences within 10%.

In practice, it is recommended that the embedded steel column should be placed along the entire height of shear walls to not only facilitate the construction process but enhance the ductility of walls. The diameter and spacing of stirrups in a range of one quarter of storey height should be increased to enhance the load-bearing capacity of connections. The embedded steel column with very small section height should be avoided. Face bearing plates (FBP) should be placed at the interface of the reinforced concrete wall and steel coupling beam to enhance the confining effect on the concrete in the joint and the load-bearing capacity of the connection.

In practice, a safety factor of 1.3 is recommended for the design strength of the connection to ensure that the yielding of the coupling beam occurs before the failure of the connection. On the other hand, the bending strength of the embedded column should be designed larger than that of the coupling beam. A safety factor of 1.1 can be used. In addition, a beneficial effect from the compressive forces in embedded column is not considered for determining the ultimate capacity of the connection, which will further increase the safety margin. For the detailing measurements. Stiffening ribs should be arranged in the embedded portion of coupling beams. The stirrups in the connection region should have a spacing no more than 150mm and diameter no less than that at the end of the wall.

Acknowledgments

The work presented in this paper was supported the Twelve-Five Science and Technology Support Program

with grant 2012BAJ13B02.

References

- ASCE (2010), Recommendations for seismic design of hybrid coupled wall systems; Technical Committee on Composite Construction of the Structural Engineering Institute, Reston, VA, USA.
- ASCE (2010), Recommendations for seismic design of hybrid coupled wall systems; Technical Committee on Composite Construction of the Structural Engineering Institute. Reston, VA, USA.
- Bengar, H.A. and Aski, R.M. (2016), "Performance based evaluation of RC coupled shear wall system with steel coupling beam", *Steel Compos. Struct., Int. J.*, **20**(2), 337-355.
- Chan-Anan, W., Leelataviwat, S. and Goel, S. (2016), "Performance-based plastic design method for tall hybrid coupled walls", *The Struct. Des. Tall Special Build.*, **25**(14), 681-699.
- El-Tawil, S., Harries, K.A., Fortney, P.J., Shahrooz, B.M. and Kurama, Y. (2010), "Seismic design of hybrid coupled wall systems: state of the art", *J. Struct. Eng.*, **136**(7), 755-769.
- Eljadei, A. (2012), "Performance based design of coupled wall structures", Ph.D. Dissertation; University of Pittsburgh, Pittsburgh, PA, USA.
- Eljadei, A. and Harries, K.A. (2014), "Design of coupled wall structures as evolving structural systems", *Eng. Struct.*, **73**, 100-113.
- Fortney, P.J., Shahrooz, B.M., Gian, A. and Rassati, G.A. (2007), "Seismic performance evaluation of coupled core walls with concrete and steel coupling beams", *Steel Compos. Struct., Int. J.*, **7**(4), 279-301.
- GB (2010), Code for design of concrete structures, GB 50010; China Architecture and Building Press, Beijing, China.
- Gholhaki, M. and Ghadaksaz, M.B. (2016), "Investigation of the link beam length of a coupled steel plate shear wall", *Steel Compos. Struct., Int. J.*, **20**(1), 34-41.
- Harries, K.A., Mitchell, D., Redwood, R.G. and Cook, W.D. (1998), "Nonlinear seismic response predictions of walls coupled with steel and concrete beams", *Can. J. Civ. Eng.*, **25**(5), 803-818.
- Hosseini, M., Sadeghi, H. and Habiby, S.A. (2011), "Comparing the nonlinear behaviors of steel and concrete link beams in coupled shear walls system by finite element analysis", *Procedia Eng.*, **14**, 2864-2871.
- Hung, C. and Lu, W. (2015), "Towards achieving the desired seismic performance for hybrid coupled structural walls", *Earthq. Struct.*, **9**(6), 1251-1272.
- JGJ (2002), Technical specification for steel reinforced concrete composite structures, JGJ 138; China Architecture and Building Press, Beijing, China.
- Kriz, L.B. and Rath, C.H. (1965), "Connection in precast concrete structures—shear strength of column heads", *PCI Journal*, **8**(6), 16-35.
- Kurama, Y. and Shen, Q. (2004), "Post-tensioned hybrid coupled walls under lateral loads", *J. Struct. Eng.*, **130**(2), 297-309.
- Li, G.Q., Gu, F.L., Jiang, J. and Sun, F.F. (2016), "Seismic behavior of steel beam-concrete wall connections with embedded steel columns (I): Experimental study", *Steel Compos. Struct., Int. J.* [Submitted]
- Morelli, F., Manfredi, M. and Salvatore, W. (2016), "An enhanced component based model for steel connection in a hybrid coupled shear wall structure: Development, calibration and experimental validation", *Comput. Struct.*, **176**, 50-69.
- Nie, J., Hu, H. and Eatherton, M. (2014), "Concrete filled steel plate composite coupling beams: Experimental study", *J. Constr. Steel Res.*, **94**, 49-63.
- Park, W.S. and Yun, H.D. (2005), "Seismic behavior of coupling beams in a hybrid coupled shear walls", *J. Constr. Steel Res.*, **61**(11), 1492-1524.
- Park, W.S. and Yun, H.D. (2006a), "Seismic performance of steel coupling beam connections in panel shear failure", *J. Constr. Steel Res.*, **62**(10), 1016-1025.
- Park, W.S. and Yun, H.D. (2006b), "Bearing strength of steel coupling beam connections embedded reinforced concrete shear walls", *Eng. Struct.*, **28**(9), 1319-1334.
- Parra-Moniesinos, G. and Wight, J. (2001), "Modeling shear behavior of hybrid RCS beam-column connections", *J. Struct. Eng.*, **127**(1), 3-11.
- Ren, X.D. and Li, J. (2015), "Calculation of concrete damage and plastic deformation", *Build. Struct.*, **15**(6), 440-444.
- Shahrooz, B.M., Tunc, G. and Deason, J.T. (2004), "Outrigger beam-Wall connections: Part II—Subassembly testing and further modeling enhancements", *J. Struct. Eng.*, **130**(2), 262-270.
- Sheikh, T., Deierlein, G., Yura, J. and Jirsa, J. (1989), "Beam-column moment connections for composite frames: Part 1", *J. Struct. Eng.*, **115**(11), 2858-2876.
- Shen, H.X. (2007), "Research on static behavior of reinforced concrete column-steel beam (RCS) moment joint", Ph.D. Dissertation; Xi'an University of Architecture and Technology, Xi'an, China.
- Shi, Y., Su, M.Z. and Mei, X.J. (2013), "Experimental study on seismic behavior of hybrid coupled wall system with steel boundary elements", *J. Earthq. Eng. Eng. Vib.*, **33**(3), 133-139.
- Wu, Y.T., Dai, C.M. and Zhou, Z.L. (2014), "Seismic behavior of shear dominant bolted endplate steel coupling beam of composite coupled shear wall", *J. Build. Struct.*, **35**(4), 255-261.
- Xuan, G., Shahrooz, B.M., Harries, K.A. and Rassati, G.A. (2008), "A performance-based design approach for coupled core wall systems with diagonally reinforced concrete coupling beams", *Adv. Struct. Eng.*, **11**(3), 265-280.
- Zhang, X.L. (2008), "Research on design method of composite frame joint consisting of steel beam and reinforced concrete column", Ph.D. Dissertation; Xi'an University of Architecture and Technology, Xi'an, China.
- Zhang, J., Wang, Q.Y., Hu, S.Y. and Wang, C. (2008), "Parameters Verification of Concrete Damaged Plastic Model of ABAQUS", *Build. Struct.*, **38**(8), 127-130.
- Zhu, H. (2008), "Experimental study and analysis on bearing capacity of connection between steel coupling beam and concrete shear wall", Ph.D. Dissertation; Central South University, Changsha, China.

CC